Journal of Catalysis **194,** 424–430 (2000)
doi:10.1006/jcat.2000.2957, available online at http://www.idealibrary.com on IDEAL®

CO_2 Reforming of Methane to Synthesis Gas over Sol–Gel-made Ni/γ-Al_2O_3 Catalysts from Organometallic Precursors

S. Tang,* L. Ji,*,† J. Lin,*,[1] H. C. Zeng,† K. L. Tan,* and K. Li‡

*Surface Science Laboratory, Department of Physics, and †Department of Chemical Engineering, National University of Singapore, 10 Kent Ridge Crescent, Singapore 119260; and ‡Institute of Materials and Research Engineering, 3 Research Link, Singapore 117602

Received March 5, 2000; revised May 22, 2000; accepted May 25, 2000

Three Ni-based catalysts with the same nickel content (10 wt%) were prepared by conventional impregnation of commercial γ-Al_2O_3 support ($NiAl_{CO\text{-}IM}$), sol–gel-made γ-Al_2O_3 ($NiAl_{SG\text{-}IM}$) and direct sol–gel processing from organometallic compounds ($NiAl_{SG}$), respectively. Their catalytic activity and coking resistivity for CO_2 reforming of methane to synthesis gas were studied in a continuous-flow microreactor under atmospheric pressure. Although three catalysts had comparable activity, they showed a great difference in coking resistivity. $NiAl_{SG\text{-}IM}$ catalyst had excellent coking resistivity with no obvious coke observed even after 80 h of reaction on stream, under thermodynamically severe conditions ($CO_2/CH_4 = 0.88$, 700°C). A little coke deposited on $NiAl_{SG}$, with an average coking rate of 0.003 g(carbon) g(cat.)$^{-1}$ h^{-1}. However, fast and heavy coke deposition occurred on $NiAl_{CO\text{-}IM}$ catalyst, with an average coking rate of 0.095 g(carbon) g(cat.)$^{-1}$ h^{-1}, and the reaction was sustained only about 3.5 h accompanied with the plugging of reactor. $NiAl_{SG\text{-}IM}$ catalyst prepared from organometallic compounds possesses very high BET surface area and small metallic Ni particles. The small size of metallic Ni particles is a key factor to prevent coke formation and the critical size of Ni particles to inhibit coke deposition is suggested to be about 10 nm. γ-Al_2O_3 support made from sol–gel processing of organometallic precursors may also play some role to prevent coke formation.

Key Words: **sol–gel Ni/γ-Al_2O_3; CO_2 reforming of methane; synthesis gas; TEM; coking resistivity.**

INTRODUCTION

In recent years CO_2 reforming of methane to synthesis gas has attracted great interest since it produces high CO/H_2 ratio synthesis gas suitable for the synthesis of higher hydrocarbons and oxygenated derivatives. Environmental protection also stimulates additional interest because both CO_2 and CH_4 are claimed to be "greenhouse gases" (1). Additionally, CO_2 reforming of methane is regarded as a potential route to store and transmit energy due to its strong endothermic effect (2, 3).

Except for osmium, all of the group VIII metals have been studied for CO_2 reforming of methane. Ferrous metals Fe (4), Co (2, 5), Ni (6–8), and noble metals (9–13) have all been reported to be active for CO_2 reforming of methane. Rostrup-Nielsen and Hansen (14) found that the catalytic activity for CO_2 reforming of methane followed the order of $Ru > Rh > Ni \approx Ir > Pt > Pd$. Although noble metals have been proved to be insensitive to coke (15, 16), the high cost and restricted availability limit their use in this process. It is therefore valuable to develop stable Ni-based catalysts.

The effects of supports (17–19) and additives (20–24) on the coke formation and stability of Ni-based catalysts were extensively investigated. Ruchenstein and Hu (17, 18) examined NiO/alkaline-earth oxide catalysts. The reduced NiO/MgO showed higher CH_4 conversion and selectivity than other catalysts. NiO/MgO had excellent stability and good resistivity to coking, which was partially ascribed to the inhibition of CO disproportionation due to the formation of a solid solution between NiO and MgO. Borowiecki and Golebiowski (20) reported that the addition of molybdenum and tungsten into the nickel-based catalysts reduced carbon deposition while keeping the same catalytic activity for CO_2 reforming of methane. Zhang and Verykios (21) found that the addition of CaO in the support ($CaO/Al_2O_3 = 1/9$) improved the stability of a 17 wt% Ni/γ-Al_2O_3 catalyst. It was suggested that the CaO promoter enhanced reactivity of the carbons formed under reforming reaction conditions and thus lowered the amount of the accumulated carbons and improved the catalyst stability. Similarly, Goula *et al.* (23) observed that the ratio of CaO to Al_2O_3 in 5 wt% Ni/CaO-Al_2O_3 catalysts had an obvious influence on the amount and reactivity of carbon species formed during CO_2 reforming of methane. The catalyst with $CaO/Al_2O_3 = 1/2$ had better coking resistivity and slightly higher catalytic activity than that with $CaO/Al_2O_3 = 12/7$. This was attributed to the effects of support composition on the morphology and particle size distribution of nickel metal. Chang *et al.* (24) also showed that the addition of alkaline promoters, such as K and Ca oxides, onto pentasil-type zeolite-supported Ni catalysts remarkably inhibited coke deposition for CO_2 reforming of

[1] To whom correspondence should be addressed. Fax: 65-7776126. E-mail: phylinjy@nus.edu.sg.

0021-9517/00 $35.00

methane, owing to the favorable adsorption of CO_2 on the surface sites neighboring Ni.

The preparation method of catalysts has significant effect on catalytic activity and coking resistivity for methane conversion to synthesis gas. Hayakawa *et al.* found that $Ni/Ca_{0.8}Sr_{0.2}TiO_3$ and $Ni/BaTiO_3$ catalysts prepared by "solid-phase crystallization" (SPC) had higher activity and better stability than those prepared by impregnation (25–27). However, the effect of support preparation, especially from organometallic precursors, has seldom been studied. In the present work, $Ni/\gamma\text{-}Al_2O_3$ catalysts, prepared by sol–gel processing from organometallic compounds and by impregnating commercial $\gamma\text{-}Al_2O_3$ respectively, have been investigated for CO_2 reforming of methane. The catalysts have also been characterized by BET surface area measurement, TPR, XRD, XPS, and TEM.

METHODS

Preparation of Catalysts

Three Ni-based catalysts, named as $NiAl_{SG}$, $NiAl_{SG\text{-}IM}$, and $NiAl_{CO\text{-}IM}$, were prepared by different methods. $NiAl_{SG}$ catalyst was prepared by sol–gel processing from organometallic precursors according to the following procedure: 10 mmol of aluminum tri-*sec*-butoxide (ASB, ACTOS, 97%) was dissolved in 150 mmol of isopropanol (Fisher Scientific, 99.9%), and then 5 mmol of acetylacetone (Merck, 99.5+%) was added as chelating agent under a nitrogen atmosphere. The precursor solution was vigorously stirred at room temperature for 30 min. Nickel nitrate dissolved in about 60 mmol of deionized water was added drop by drop under mild stirring. The sample gelled in a few minutes. The resulting transparent and green gel was aged for 5 days at room temperature and dried at 60°C for another 5 days. It was then calcined at 600°C for 5 h. $NiAl_{SG\text{-}IM}$ and $NiAl_{CO\text{-}IM}$ catalysts were prepared by incipient wetness impregnation. The $\gamma\text{-}Al_2O_3$ support of $NiAl_{SG\text{-}IM}$ was synthesized following the above sol–gel procedure, but only 60 mmol of deionized water without nickel nitrate was added during the sol–gel processing. The $NiAl_{CO\text{-}IM}$ employed commercial $\gamma\text{-}Al_2O_3$ (Merk) as its support. The samples were also calcined at 600°C for 5 h. The loading of nickel was 10 wt% for all three catalysts.

Evaluation of Catalytic Activity and Coke Deposition

The catalytic activity was evaluated on a continuous-flow quartz microreactor (i.d. 4 mm), under atmospheric pressure. One hundred milligrams of catalyst (35–50 mesh size) was loaded for each test. The catalysts were reduced in a flow of H_2 (30 ml/min) at 700°C for 1 h before a premixed feed gas (19.8% CH_4/17.5% CO_2/Ar) was introduced into the catalyst bed. The outlet gas composition was measured by gas chromatography. The yield of CO is defined as the mole ratio of $CO/(CH_4 + CO + CO_2)$ in the effluent gas. The measurement of coke deposited on the reacted catalysts followed procedures similar to those previously described in detail (28). Briefly, after reaction the catalyst sample was cooled to 50°C in a flow of He and temperature-programmed oxidation (TPO) was carried out in a 10% O_2/Ar gas stream with temperature linearly increased from 50 to 800°C at a rate of 15°C/min. The CO_2 and CO produced were detected by an on-line mass spectrometer that was calibrated by monitoring the decomposition of weighted amount of calcium carbonate.

Characterization of Catalysts

The BET surface area of the as-prepared catalysts was measured on a Micromeritics sorption analyzer (model ASAP2400), using N_2 as the adsorbate at 77 K.

Temperature-programmed reduction (TPR) was carried out in the following procedure. The sample (100 mg) was heated from room temperature to 750°C in a He flow until no desorption gases were detected. The sample was then cooled to room temperature and the carrier gas was replaced by 10% H_2/Ar, at a flow rate of 45 ml/min. A linear increase of temperature from room temperature to 820°C, at a rate of 15°C/min, was adopted. The amount of consumed H_2 was measured using a thermal conductivity detector connected to a recorder.

A Philips PW 1710 X-ray diffraction spectrometer with a Cu $K\alpha$ radiation source was utilized to detect the crystalline phases of catalysts.

X-ray photoelectron spectra were acquired with a VG ESCALAB MK II spectrometer, using an Al $K\alpha$ radiation (1486.6 eV, 120 W). Analyzer pass energy of 20 eV was adopted for all narrow scans. The C 1*s* peak at binding energy of 284.6 eV due to adventitious carbon was used as an internal reference.

Transmission electron microscopy (TEM) was performed on a Jeol system with a tension voltage of 100 kV. High-resolution electron microscopy (HREM) was carried out on a Philips CM 300 with a tension voltage of 300 kV, FEG emission, and UT objective lens.

RESULTS AND DISCUSSION

Characterization of Catalysts

The BET surface area and the size of metallic Ni particles are given in Table 1. The BET surface areas followed the order of $NiAl_{SG} > NiAl_{SG\text{-}IM} \gg NiAl_{CO\text{-}IM}$. $NiAl_{SG}$, which was prepared from organometallic precursors by sol–gel processing, had a very high surface area of 183.2 $m^2 g^{-1}$ while $NiAl_{CO\text{-}IM}$ was 90.9 $m^2 g^{-1}$, only about half of the former. The average size of metallic Ni particles in $NiAl_{SG\text{-}IM}$ (8.2 nm from TEM) was much smaller than that in $NiAl_{CO\text{-}IM}$ (26 nm). The TEM micrograph of $NiAl_{CO\text{-}IM}$,

TABLE 1

BET Surface Areas and the Size of Metallic Ni Particles Estimated from XRD and TEM Measurements

Catalysts	Surface area (m^2/g)	Average size of metallic Ni (nm)[a]	
		XRD	TEM
$NiAl_{SG}$	183.2	NA	—
$NiAl_{SG\text{-}IM}$	171.1	9.9	8.2
$NiAl_{CO\text{-}IM}$	90.9	24	26

[a] Samples after TPR up to 820°C; NA, not detectable.

presented in Fig. 1A, illustrates large metallic Ni particles. The very small metallic Ni particles in $NiAl_{SG\text{-}IM}$ catalyst were viewed by HREM, as shown in Fig. 1B. The approximate size of metallic Ni particles was also obtained by XRD measurement. The XRD patterns of the reduced catalysts are displayed in Fig. 2. The peak of metallic Ni at $2\theta = 44.4°$ in $NiAl_{CO\text{-}IM}$ was sharp and narrow whereas it was weak

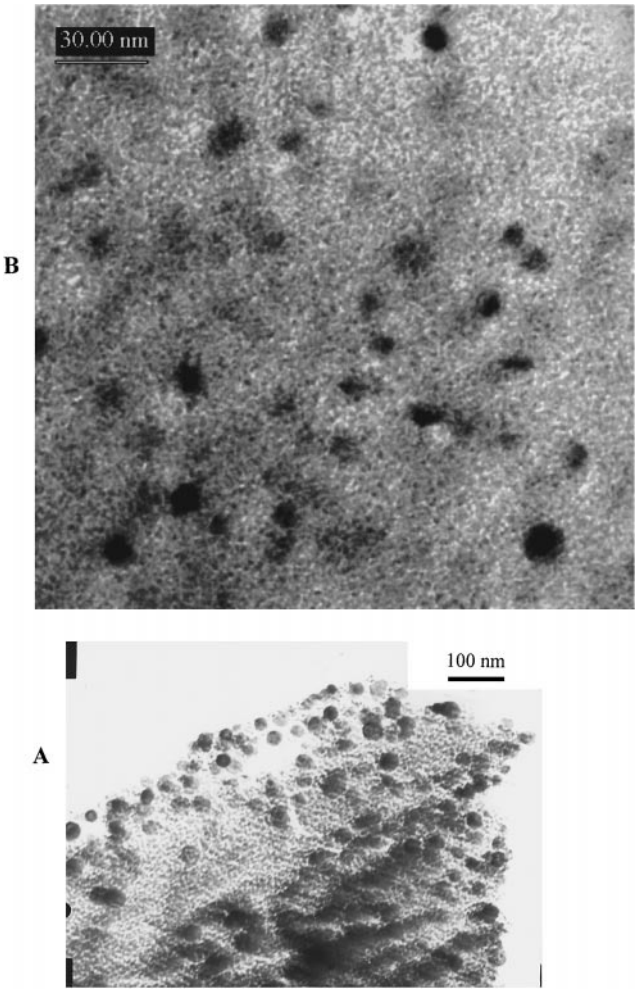

FIG. 1. TEM micrographs of the reduced catalysts illustrating the morphology of Ni particles: (A) $NiAl_{CO\text{-}IM}$; (B) $NiAl_{SG\text{-}IM}$.

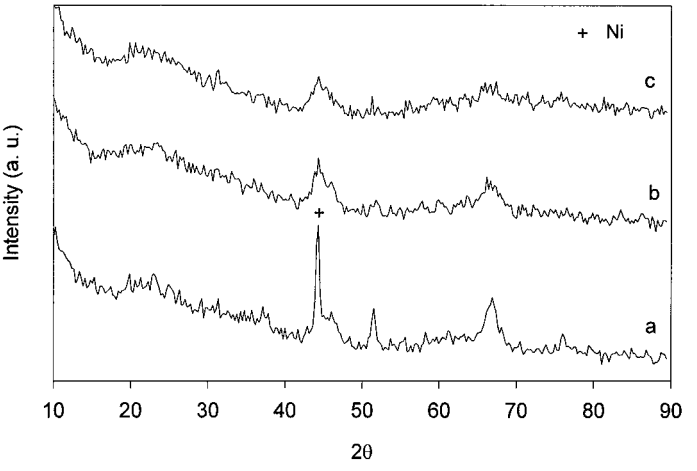

FIG. 2. XRD patterns of the reduced catalysts: (a) $NiAl_{CO\text{-}IM}$; (b) $NiAl_{SG\text{-}IM}$; (c) $NiAl_{SG}$.

and broad in $NiAl_{SG\text{-}IM}$. It is noted that a very weak and broad peak near $2\theta = 44.4°$ was also visible on $NiAl_{SG}$ (see Fig. 1C), but it was near the peak width limit of XRD and the size of nickel particles could not be calculated. It is unexpected that the crystallization of Ni in $NiAl_{SG}$ catalyst did not seem good and a part of the Ni might be amorphous as observed by HREM (not shown). This reveals the small metallic Ni particles and their higher dispersion in $NiAl_{SG\text{-}IM}$, as compared to those in $NiAl_{CO\text{-}IM}$. Since both $NiAl_{SG\text{-}IM}$ and $NiAl_{CO\text{-}IM}$ were prepared by the same impregnation method, the properties of the small metallic Ni particles in $NiAl_{SG\text{-}IM}$ should be closely related to the properties of its support made from organometallic precursors, such as the very high BET surface area.

The temperature-programmed reduction profiles of catalysts are given in Fig. 3. All three catalysts have a single reduction peak, but with a little different maximum

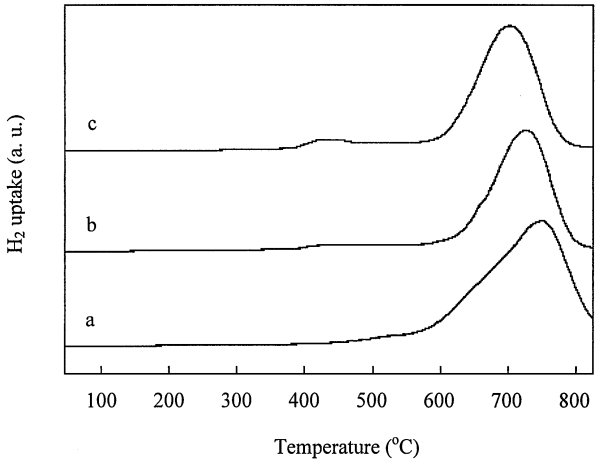

FIG. 3. TPR profiles of catalysts: (a) $NiAl_{CO\text{-}IM}$; (b) $NiAl_{SG\text{-}IM}$; (c) $NiAl_{SG}$.

peak temperatures at 748, 718, and 695°C for $NiAl_{CO\text{-}IM}$, $NiAl_{SG\text{-}IM}$, and $NiAl_{SG}$, respectively. This appears to indicate that the strength of the metal–support interaction decreases in the order of $NiAl_{CO\text{-}IM} > NiAl_{SG\text{-}IM} > NiAl_{SG}$, though the difference is not large.

XPS was used to analyze the valence state of elements and surface composition of catalysts. Ni $2p_{3/2}$ XPS spectra of the as-prepared catalysts are presented in Fig. 4. The Ni $2p_{3/2}$ peak in $NiAl_{CO\text{-}IM}$ catalyst is centered at a binding energy of 855.2 eV, with a shake-up peak at 861.2 eV (Fig. 4a), which could be identified as Ni^{2+}. The peaks shift to 855.6 eV and 861.7 eV respectively for both $NiAl_{SG\text{-}IM}$ and $NiAl_{SG}$ (Figs. 4b and 4c). After H_2 reduction, Ni^0 is detected at 852.2 eV, but the Ni^{2+} peak at 855.6 eV is still predominant for all three reduced catalysts (Fig. 5). The satellite peaks become weak due to the decrease of Ni^{2+} by reduction. Actually three reduced catalysts have also identical O 1*s* and Al 2*p* XPS spectra, with the binding energies of 530.8 eV and 74.0 eV respectively (not shown). This reveals no obvious difference in electronic structure among the three reduced catalysts.

However, a remarkable difference in surface composition was found for three catalysts, as indicated by the Ni/Al mole ratios in Table 2. The Ni/Al mole ratio on the surface of $NiAl_{SG}$ is close to that of $NiAl_{SG\text{-}IM}$ for both the as-prepared and reduced samples. After reduction, the Ni/Al mole ratios decreased a little for these two catalysts. In contrast, the Ni/Al mole ratio (0.38) was relatively high on the surface of the as-prepared $NiAl_{CO\text{-}IM}$. The ratio in the reduced $NiAl_{CO\text{-}IM}$ (0.41) increased a little. It should be mentioned that the total Ni/Al mole ratio based on the weight percentage of catalysts (10 wt% of Ni loading) is 0.097. The total Ni/Al mole ratio includes the surface and bulk of the catalysts. If the dispersion of the metal is high and the distribution of the metal particles on the supports is uniform, the surface Ni/Al mole ratio should be close to the total Ni/Al mole ratio (29). This indicates that nickel segregation occurs on the surfaces of all three catalysts, in particular on the $NiAl_{CO\text{-}IM}$ surface.

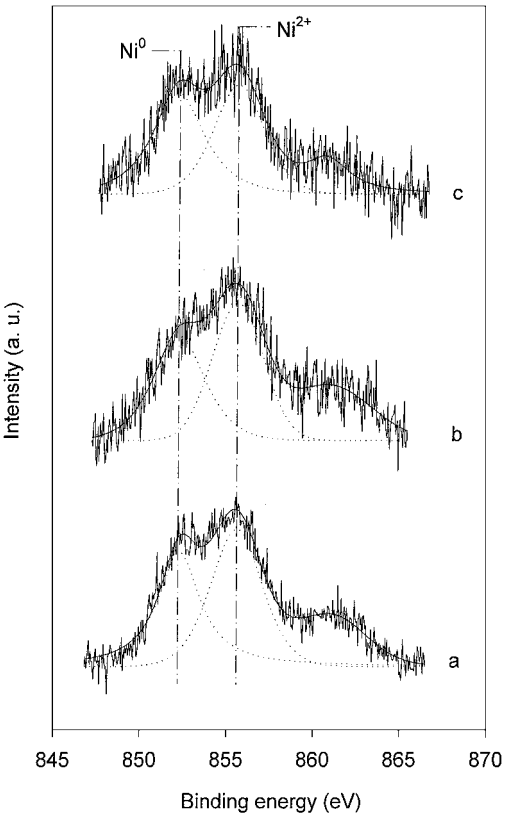

FIG. 5. Ni $2p_{3/2}$ XPS spectra of the reduced catalysts: (a) $NiAl_{CO\text{-}IM}$; (b) $NiAl_{SG\text{-}IM}$; (c) $NiAl_{SG}$.

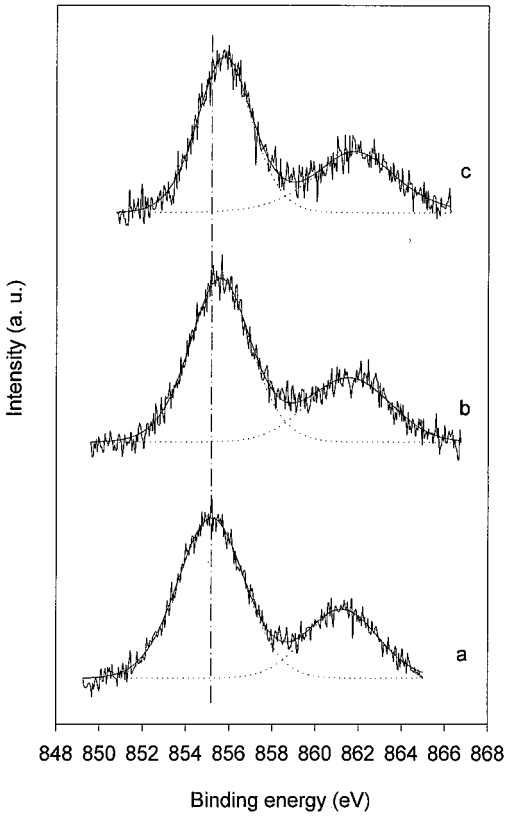

FIG. 4. Ni $2p_{3/2}$ XPS spectra of the as-prepared catalysts: (a) $NiAl_{CO\text{-}IM}$; (b) $NiAl_{SG\text{-}IM}$; (c) $NiAl_{SG}$.

TABLE 2

Ni/Al Mole Ratios on the Surface of Catalysts Derived from XPS

Catalysts	Ni/Al mole ratio	
	As-prepared	After reduction
$NiAl_{SG}$	0.23	0.18
$NiAl_{SG\text{-}IM}$	0.21	0.18
$NiAl_{CO\text{-}IM}$	0.38	0.41

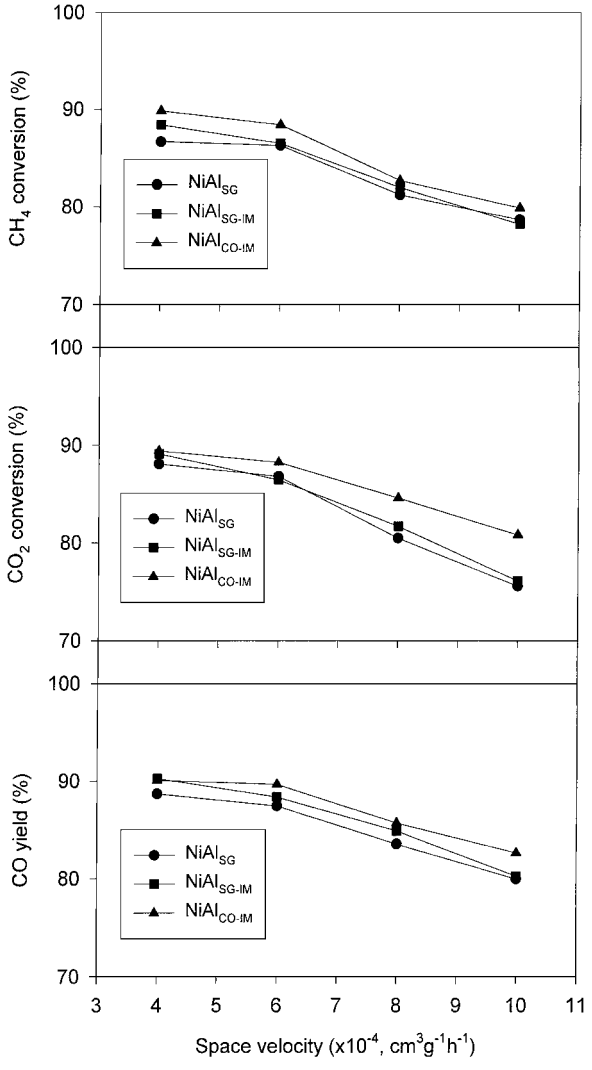

FIG. 6. Effect of space velocity on CH_4, CO_2 conversion and CO yield (feed gas, 19.8% CH_4/17.5% CO_2/Ar; 700°C).

Catalytic Activity and Coke Deposition

Figure 6 presents the effect of space velocity on catalytic activity of three catalysts, at 700°C. As expected, CH_4, CO_2 conversion and CO yield decreased with the increase of space velocity. $NiAl_{SG}$ and $NiAl_{SG\text{-}IM}$ catalysts had similar methane and CO_2 conversion whereas $NiAl_{CO\text{-}IM}$ showed a little higher methane and CO_2 conversion in the range of space velocity of $(4–10) \times 10^4$ cm^3 g^{-1} h^{-1}. Nevertheless, CO yields were comparable for three catalysts. It is generally expected that the better the dispersion of active metal component, for example, the smaller the metallic Ni particles in $NiAl_{SG\text{-}IM}$ catalyst, the higher is its catalytic activity. Although the dispersion of metal Ni in $NiAl_{SG}$ and $NiAl_{SG\text{-}IM}$ catalysts is higher than that in $NiAl_{CO\text{-}IM}$, as revealed by TEM, XRD, and XPS analysis, their catalytic activity is comparable. This result may be related to two factors. One is that under our integral operating conditions, the measurement is not far enough from equilibrium conversion, even at very high space velocity (1×10^5 cm^3 g^{-1} h^{-1}). Under differential reaction conditions and at very low conversion, a large difference in activity would be expected. As will be demonstrated in the next paragraph, the other is that the fast coking on $NiAl_{CO\text{-}IM}$ catalyst makes its activity relatively high. Due to fast coking, it is difficult to measure activity of $NiAl_{CO\text{-}IM}$.

However, a large difference in their resistance to coke formation was found (see Table 3). No coke deposition on $NiAl_{SG\text{-}IM}$ catalyst occurred after 4 h of reaction. A little coke with an average coking rate of 0.003 g(carbon) g^{-1}(cat.) h^{-1} was observed on $NiAl_{SG}$ but a large amount of coke, with an average coking rate of 0.095 g(carbon) g^{-1}(cat.) h^{-1}, was deposited on $NiAl_{CO\text{-}IM}$ and caused the plugging of the reactor within 3.5 h of reaction. A little higher CH_4 and CO_2 conversion over $NiAl_{CO\text{-}IM}$ may thus result from significant coke deposition, as shown in Fig. 6, since coke deposition was not included in the calculation of catalytic activity.

Long-time stability of $NiAl_{SG\text{-}IM}$ catalyst was further examined. After 80 h of continuous reaction at 700°C, $NiAl_{SG\text{-}IM}$ catalyst did not show any deactivation (see Fig. 7) and kept its original particle shape with no shattering of catalyst. It is worth mentioning that a negligible amount of coke was formed, especially under thermodynamically severe conditions employed in this test ($CO_2/CH_4 = 0.88 < 1$, 700°C). So sol–gel-made $NiAl_{SG\text{-}IM}$ catalyst has manifested itself as an excellent catalyst for CO_2 reforming of methane, with both good catalytic activity and long-time stability.

In contrast, a large amount of coke deposition on $NiAl_{CO\text{-}IM}$ led to the shattering of catalyst and the plugging of reactor after only 3.5 h reaction. The main type of coke is tubular whisker carbon, as revealed by the TEM micrograph in Fig. 8A. The diameter of the nanotube is in the range of 10–35 nm. Since Ni particles at the extremity of carbon filaments are still accessible to reactants, whisker carbon has been found not to affect the catalytic activity of catalyst (30), as observed on $NiAl_{CO\text{-}IM}$ catalyst. But it is necessary to avoid the formation of whisker carbon because

TABLE 3

Average Coking Rates on Three Catalysts for CO_2 Reforming of Methane (Feed Gas: 19.8% CH_4/17.5% CO_2/Ar; GHSV = 4×10^4 cm^3 g^{-1} h^{-1}, 700°C)

Catalysts	Average coking rate (g(carbon) g^{-1}(cat.) h^{-1})
$NiAl_{SG}$	0.003[a]
$NiAl_{CO\text{-}IM}$	0.0[a]
$NiAl_{CO\text{-}IM}$	0.095[b]

[a] Reaction time = 4 h.
[b] Reaction time = 3.5 h due to the plugging of reactor.

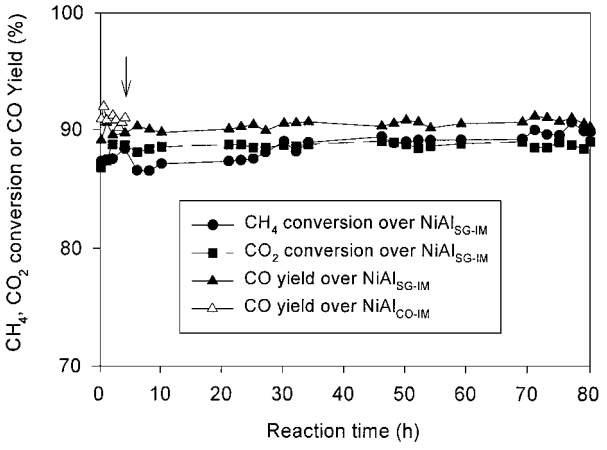

FIG. 7. Change of catalytic activity as a function of time over $NiAl_{SG-IM}$ and $NiAl_{CO-IM}$ catalysts. ↓ Symbol indicates that the reaction on $NiAl_{CO-IM}$ was interrupted at 3.5 h owing to the plugging of reactor by carbon deposition (feed gas, 19.8% CH_4/17.5% CO_2/Ar, GHSV = 4×10^4 cm^3 g^{-1} h^{-1}, 700°C).

it will destroy the catalyst texture and structure and cause the shattering of catalyst. The topography of $NiAl_{CO-IM}$ catalyst after 80 h of reaction is observed by HREM and shown in Fig. 8B. The sintering of metallic Ni occurred and metallic Ni particles grew up to 28 nm.

Discussion on Coking Resistivity

Three catalysts showed comparable activity for CO_2 reforming of methane to synthesis gas, but appreciably different coking resistivity. No detectable coke was found on $NiAl_{SG-IM}$ catalyst. It is important to know what are the key factors that contribute to the prevention of coke formation on $NiAl_{SG-IM}$. The strong interaction between Ni and support is suggested to prevent coke deposition on Ni/MgO (17, 18) and Ni/La_2O_3 (31, 32) catalysts. A NiO–MgO solid solution in Ni/MgO catalyst was formed. Only a small amount of NiO was reduced to Ni and the formation of large Ni clusters was prevented. CO disproportionation was effectively inhibited by the strong interactions between the small Ni particles and MgO. The interaction between nickel and lanthanum species created a new type of synergetic sites at the Ni–La_2O_3 interfacial area (31, 32). The formed $La_2O_2CO_3$ and formate species were suggested to react with the carbon species, which decreased coke deposition. XPS analysis reveals no obvious difference in electronic structure among three catalysts, especially for the reduced catalysts (Fig. 5). Though TPR profiles in Fig. 3 illustrate that the maximum peak temperature of $NiAl_{SG-IM}$ is between those of $NiAl_{SG}$ and $NiAl_{CO-IM}$, the difference is not very large among three catalysts. The metal–support interaction is thus not a key factor that affects coke formation on three catalysts. Additionally, it seems impossible to form different intermediate species among three catalysts like Ni/La_2O_3 since they have similar chemical composition.

Nevertheless, the obvious advantage of $NiAl_{SG-IM}$ catalyst is the very small size of the metallic Ni particles, as revealed by the TEM micrograph in Fig. 1B. Lercher *et al.* suggested that the rate of whisker carbon formation is proportional to the particle size of Ni and below a critical Ni particle size (diameter <2 nm), formation of carbon slowed down dramatically (33). But Ponzi *et al.* reported that for the formation of whisker carbon the minimum diameter of the Ni particles was about 10 nm, while the minimum C/Ni ratio, i.e., carbon atoms adsorbed on superficial Ni, was 8–10 (34, 35). The observed minimum diameter of carbon nanotubes is about 10 nm on Ni-based catalysts (Fig. 8A). This may provide evidence that the critical size of Ni particle to prevent the formation of tubular whisker carbon is about 10 nm for CO_2 reforming of methane. The very small size of initial metallic Ni in $NiAl_{SG-IM}$ (average size ≈ 8.2 nm) is hence believed to be a key factor to inhibit whisker carbon formation. High surface areas of

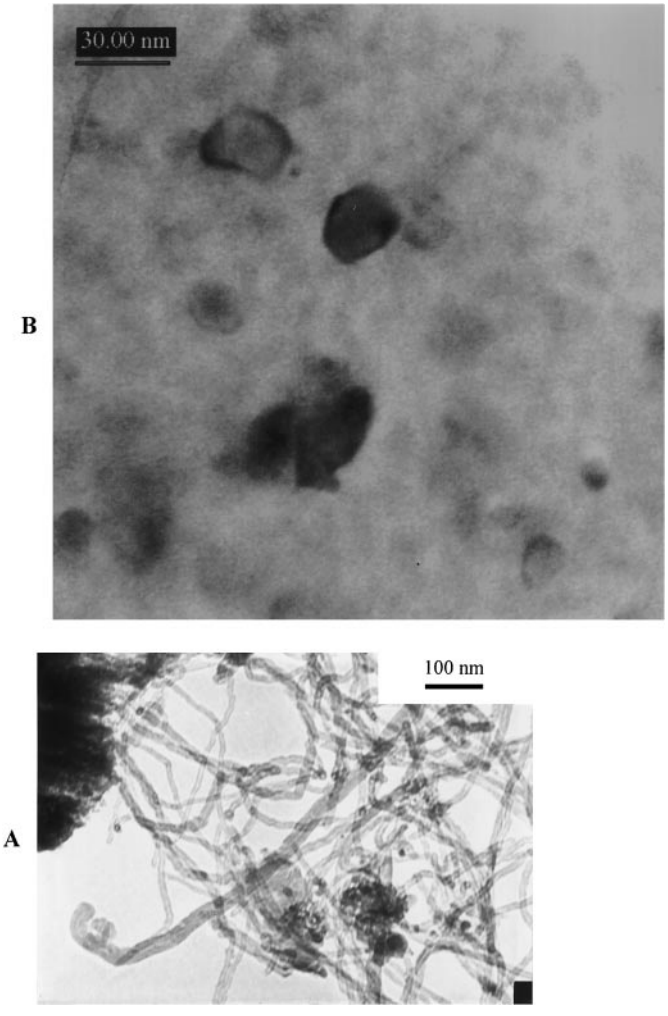

FIG. 8. TEM micrographs of the reacted catalysts: (A) morphology of coke deposited on $NiAl_{CO-IM}$; (B) morphology of Ni particles on $NiAl_{SG-IM}$ after 80 h of reaction.

sol–gel-made supports from organometallic precursors should be helpful to enhance the dispersion of the active component, like nickel in the present case, and thus prevent the segregation of nickel on the surfaces. Nichio *et al.* (30) found that Ni_{OM}/α-Al_2O_3 catalyst using Ni-acetylacetonate as a precursor compound could effectively refrain coke formation for partial oxidation of methane to synthesis gas though it had an initial size distribution similar to that of metallic Ni to Ni_{IN}/α-Al_2O_3 using $Ni(NO_3)_2$ as a precursor compound. But rapid sintering of Ni particles in Ni_{OM}/α-Al_2O_3 catalyst led to a continuous deactivation. Despite the growth of metallic Ni up to 28 nm with the extension of reaction time, carbon deposition was still negligible. sol–gel-made supports from organometallic precursors may have some roles to prevent coke formation though the mechanism is not clear. Whether $NiAl_{SG\text{-}IM}$ catalyst can afford a longer time ordeal (>80 h) needs to be further investigated because the growth of Ni particles also occurred though at a very slow rate of sintering. The same effects should be present in $NiAl_{SG}$ catalyst, but probably to a lesser extent. A little coke deposition detected on $NiAl_{SG}$ catalyst may be related to the bad crystallization of nickel. It seems better to introduce nickel by impregnation other than addition during sol–gel process.

In contrast, large initial Ni particles and segregation of nickel on the surfaces were observed over $NiAl_{CO\text{-}IM}$ catalyst. Rostrup-Nielsen pointed out that large nickel clusters were susceptible to coke deposition (36). Due to the significant segregation of nickel on the surface of support, large nickel clusters were easily formed. This would result in the rapid and heavy coke deposition on $NiAl_{CO\text{-}IM}$ catalyst.

SUMMARY

Ni-based catalysts supported on the commercial γ-Al_2O_3 ($NiAl_{CO\text{-}IM}$) and the sol–gel-made γ-Al_2O_3 ($NiAl_{SG\text{-}IM}$ and $NiAl_{SG}$) from organometallic precursors have showed almost identical catalytic activity for CO_2 reforming of methane to synthesis gas under integral reaction conditions. But a substantial difference in coking resistivity and stability between these two kinds of catalysts has been observed. A fast and heavy coke deposition on $NiAl_{CO\text{-}IM}$ catalyst led to its shattering and the interruption of reaction process in only 3.5 h whereas coke deposition on $NiAl_{SG\text{-}IM}$ was negligible and catalytic activity kept unchanged for CO_2 reforming of methane even after 80 h of reaction on stream.

The outstanding performance and excellent coking resistivity of $NiAl_{SG\text{-}IM}$ catalyst have been found to be greatly related to the small size of initial Ni particles and the high dispersion of nickel that should be ascribed to the high BET surface area of sol–gel-made supports. The γ-Al_2O_3 supports prepared from organometallic precursors may also be beneficial to prevent coke formation. In addition, it seems better to introduce the active component nickel by impregnation rather than addition during sol–gel processing.

REFERENCES

1. Delmon, B., *Appl. Catal. B* **1**, 139 (1992).
2. McCrary, J., McCrary, G. E., Chubb, T. A., Nemecek, J. J., and Simmons, D. E., *Sol. Energy* **29**, 141 (1982).
3. Fish, J. D., and Hawn, D. C., *J. Sol. Energy Eng.* **109**, 215 (1987).
4. Sodesawa, T., Dogash, A., and Nozaki, F., *React. Kinet. Catal. Lett.* **11**, 149 (1991).
5. Tang, S., Lin, J., and Tan, K. L., *Surf. Interface Anal.* **28**, 155 (1999).
6. Guerrero-Ruiz, A., Rodrigues-Ramos, I., and Sepulveda-Escribano, A., *J. Chem. Soc., Chem. Commun.* 487 (1993).
7. Gadalla, A. M., and Sommer, M. E., *J. Am. Ceram. Soc.* **72**, 683 (1989).
8. Gadalla, A. M., and Sommer, M. E., *Chem. Eng. Sci.* **44**, 2825 (1989).
9. Yamazaki, O., Nozaki, T., Omata, K., and Fujimoto, K., *Chem. Lett.* 1953 (1992).
10. Richardson, J. T., and Paripatyadar, S. A., *Appl. Catal.* **61**, 293 (1990).
11. Solymosi, F., Kutsan, G., and Erdohelyi, A., *Catal. Lett.* **11**, 14 (1991).
12. Perera, J. S. H. Q., Couves, J. W., Sankar, G., and Thomas, J. M., *Catal. Lett.* **11**, 219 (1991).
13. Ashcroft, A. T., Cheetham, A. K., Green, M. L. H., and Vernon, P. D. F., *Nature* **352**, 225 (1991).
14. Rostrup-Nielsen, J. R., and Hansen, J. H. H., *J. Catal.* **144**, 38 (1993).
15. Bradford, M. C. J., and Vannice, M. A., *J. Catal.* **173**, 157 (1998).
16. Tang, S., Lin, J., and Tan, K. L., *Catal. Lett.* **59**, 129 (1999).
17. Ruchenstein, E., and Hu, Y. H., *Appl. Catal. A* **133**, 149 (1995).
18. Hu, Y. H., and Ruchenstein, E., *Catal. Lett.* **36**, 145 (1996).
19. Bradford, M. C. J., and Vannice, M. A., *Appl. Catal. A* **142**, 73 (1996).
20. Borowiecki, T., and Golebiowski, A., *Catal. Lett.* **25**, 309 (1994).
21. Zhang, Z. L., and Verykios, X. E., *Catal. Today* **21**, 589 (1994).
22. Choi, J. S., Moon, K. I., Kim, Y. G., Lee, J. S., Kim, C. H., and Trimm, D. L., *Catal. Lett.* **52**, 43 (1998).
23. Goula, M. A., Lemonidou, A. A., and Efstathiou, A. M., *J. Catal.* **161**, 626 (1996).
24. Chang, J.-S., Park, S.-E., and Chon, H., *Appl. Catal. A* **145**, 111 (1996).
25. Hayakawa, T., Harihara, H., Andersen, A. G., Suzuki, K., Yasuda, H., Tsunoda, T., Hamakawa, S., York, A. P. E., Yoon, Y. S., Shimizu, M., and Takehira, K., *Appl. Catal. A* **149**, 391 (1997).
26. Shiozaki, R., Andersen, A. G., Hayakawa, T., Hamakawa, S., Suzuki, K., Shimizu, M., and Takehira, K., *J. Chem. Soc., Faraday Trans.* **93**, 3235 (1997).
27. Hayakawa, T., Suzuki, S., Nakamura, J., Uchijima, T., Hamakawa, S., Suzuki, K., Shishido, T., and Takehira, K., *Appl. Catal. A* **183**, 273 (1999).
28. Tang, S., Lin, J., and Tan, K. L., *Catal. Lett.* **51**, 169 (1998).
29. Hu, Y. H., and Ruchenstein, E., *Catal. Lett.* **43**, 71 (1997).
30. Nichio, N., Casella, M., Ferretti, O., Gonzalez, M., Nicot, C., Moraweck, B., and Frety, R., *Catal. Lett.* **42**, 65 (1996).
31. Zhang, Z. L., and Verykios, X. E., *J. Chem. Soc., Chem. Commun.* 71 (1995).
32. Zhang, Z. L., Verykios, X. E., MacDonald, S. M., and Affrossman, S., *J. Phys. Chem.* **100**, 744 (1996).
33. Lercher, J. A., Bitter, J. H., Hally, W., Niessen, W., and Seshan, K., *Stud. Surf. Sci. Catal.* **101**, 463 (1996).
34. Duprez, D., Demicheli, M. C., Marecot, P., Barbier, J., Ferretti, O. A., and Ponzi, E. N., *J. Catal.* **124**, 324 (1990).
35. Demicheli, M. C., Duprez, D., Barbier, J., Ferretti, O. A., and Ponzi, E. N., *J. Catal.* **145**, 437 (1994).
36. Rostrup-Nielsen, J. R., *J. Catal.* **85**, 31 (1984).